Dynamic Imaging Analysis of SERS-Active Nanoparticle Clusters in Suspension

Alastair W. Wark,* Robert J. Stokes, Steven B. Darby, W. Ewen Smith, and Duncan Graham*

Centre for Molecular Nanometrology, WestCHEM, Department of Pure and Applied Chemistry, University of Strathclyde, Glasgow, U.K., G1 1XL

Received: August 10, 2010; Revised Manuscript Received: September 22, 2010

A novel wide-field approach for the real-time Surface Enhanced Raman Scattering (SERS) imaging of multiple silver nanoparticle clusters suspended in solution is described. This method enables direct correlation of the SERS activity of a single nanoparticle aggregate and its size through measurement of the cluster diffusion coefficient and can also be performed in a high-throughput basis. As a first demonstration, we investigate the salt-induced aggregation of silver nanoparticles in the presence of a reporter tag molecule, which has a high affinity for the nanoparticle surface. In addition to tracking individual particles, direct comparison of Rayleigh and SERS videos of the same colloid solution enabled measurement of the fraction of individual clusters that are SERS active and the dependence of this value on the relative concentration of the tag molecule. Furthermore, given the ability to also rapidly profile any nonuniformity in particle size distributions, we expect this approach will not only provide a new tool for the fundamental understanding of SERS but also significantly contribute to the development of an array of emerging nanoparticle-enhanced biomolecule and imaging detection platforms.

Introduction

Surface enhanced Raman scattering (SERS) measurements involving the controlled assembly of metal nanoparticles in the presence of a specific target or reporter molecule has emerged in recent years as a highly promising analytical technique.[1] In addition to being capable of single molecule detection and characterization,[2,3] there is a great potential for the use of SERS in many fields including bioanalysis,[4] the fabrication of nanotags for in vivo imaging,[5,6] and explosives detection.[7] However, despite the considerable depth of literature available, the understanding of colloid-based SERS measurements and the aggregation process has still to be thoroughly addressed. This is due, in part, to the complex relationship between the local geometry of nanoparticles forming a cluster and the resulting Raman enhancement. Also, there is a lack of techniques capable of directly investigating in situ the formation and size distribution of individual clusters formed in a colloidal solution and correlating the SERS activity of each.

A variety of investigations on the SERS properties of aggregated colloid solutions have been reported. The vast majority of SERS measurements are performed in bulk with no accurate knowledge of the number density of particles in the detection volume at any one time resulting in a loss of information due to averaging.[8,9] Alternatively, spatially isolated nanoparticle clusters immobilized on a surface can be mapped to allow direct correlation between optical and TEM measurements.[10−12] However, such investigations are slow and inefficient and provide limited statistics with studies typically limited to a few tens of aggregates. Also, it is unclear to what extent the process of surface immobilization and substrate drying affects the intraparticle geometry of each cluster and its subsequent SERS activity.

Recently, a small number of groups have described solution-based approaches that enable the rapid spectral analysis of single SERS active nanoparticle tags. This involves either monitoring individual particles diffusing through a confocal laser spectrometer[13] or developing a flow cytometry-based methodology where the Raman signals of individual tags are accumulated in a high-throughput basis under continual flow.[14,15] This provides access to a wealth of information correlating simultaneously the brightness and spectral variability of the Raman response relative to the Rayleigh scattering and background behaviors for thousands of tags. However, no direct information on cluster size is obtainable. Techniques such as dynamic light scattering (DLS) do allow rapid characterization but often produce a skewed average size weighted in favor of larger particles. Furthermore, as well as being unsuitable for polydisperse samples, multiparameter investigations needed to correlate SERS activity with aggregate formation and size cannot be performed on a per particle basis using DLS.

In this article, an alternative imaging-based approach for the dynamic analysis of individual SERS active nanoparticles is introduced. We show for the first time that the SERS imaging modality can be applied in a manner comparable to conventional Rayleigh scattering[16−18] and fluorescent[19,20] imaging measurements to directly track nanoparticles at rates sufficient to determine their diffusion coefficients in biologically relevant solutions. Conventional SERS imaging measurements involve the confocal spectral mapping of surface immobilized structures and the subsequent plotting of data where each pixel corresponds to the spectral intensity at a particular wavenumber shift.[21,22] Although information-rich, this configuration cannot be readily applied to the real-time monitoring of mobile nanoparticles in situ and dual measurements of both SERS activity and diffusion coefficients of nanoparticle clusters have not been reported. The setup described in this article is relatively simple and avoids the use of spectrometer and confocal systems while maintaining good discrimination against possible background signal contributions. Furthermore, by adopting a wide-field configuration large numbers of clusters (∼100 or so) can be imaged and tracked at the same time.

As a first demonstration of dynamic SERS imaging, the salt-induced aggregation of a silver nanoparticle colloidal solution

* To whom correspondence should be addressed. E-mail: alastair.wark@strath.ac.uk (A.W.W.), duncan.graham@strath.ac.uk (D.G.).

10.1021/jp107559x © 2010 American Chemical Society
Published on Web 10/05/2010

in the presence of a strongly adsorbing reporter molecule was investigated. A methodology was developed where SERS and Rayleigh videos of the aggregated colloid were directly compared to reveal details on the fraction of clusters formed that exhibit SERS activity. In addition, the ability to track in real-time single clusters formed in solution on a high-throughput basis also provides a new route toward understanding the aggregation behavior of metallic colloids; which is an essential component of many strategies for the controlled assembly of functional nanostructures and in the design of nanoparticle-based sensors.

Experimental Section

Chemicals. All materials were purchased from Sigma-Aldrich and used without further purification unless otherwise stated. The analyte dye, 3,5-dimethoxy-4-(6′-azobenzotriazoyl)phenol, ABT-DMOP, used in the SERS measurements was synthesized as described previously.[23]

Silver nanoparticle solutions were prepared by reduction of silver nitrate with trisodium citrate according to a modification of the method reported by Lee and Meisel.[24,25] The average particle diameter measured from SEM analysis was 56 nm with a small fraction of nonspherical shapes including rods also present, which is typical of this synthesis. Using an extinction coefficient of $\varepsilon = 4 \times 10^{10}$ M^{-1} cm^{-1} at the 409 nm plasmon resonance maximum, the nanoparticle stock solution had an estimated concentration of 0.105 nM ($\sim 6 \times 10^{10}$ particles/ml). This value agrees well with direct measurements of the particle density in solution (described later) where the average number of particles imaged by Rayleigh scattering is counted within the calibrated field of view for a very dilute solution.

Bulk SERS Measurements. Ensemble-averaged spectra were acquired using a Renishaw model 100 probe system with a 514.5 nm argon ion laser and utilizing a 20× long working distance objective lens to focus the laser beam into a 1 cm cuvette containing the sample. In a typical measurement, ABT-DMOP was added at various bulk concentrations (10^{-11}−10^{-5} M) to 500 μL of Ag nanoparticle stock solution. Particle aggregation was performed by adding 10 μL of 1 M $MgSO_4$ solution. After mixing, spectra were immediately acquired with an integration time of 1 s and laser power of ~4 mW.

Dynamic SERS Imaging Measurements. A schematic of the setup used for the SERS imaging of individual nanoparticle clusters is shown in Figure 1. Briefly, a 514.5 nm laser (StellarPro, Modu-laser) is passed through a cleanup filter (ThorLabs) with a 2 nm bandwidth at half-maximum before being transmitted through a channel (3 × 4 × 15 mm) etched in a glass pyrex substrate capped at both ends with a thin glass window and with a glass window forming the channel ceiling. Prior to channel entry, the incident laser beam was passed through a PCX lens (f = 20 cm). A 20×/0.4 long-working distance objective lens was used to collect both Rayleigh and Raman images in combination with a further magnification lens placed prior to an Andor iXon+ 897 EMCCD camera. The effective field of view (134 × 134 μm) was less than the beam width at the laser focus to ensure uniform illumination. The laser power at the channel entrance was ~25 mW. When obtaining SERS images, a part of the SERS spectrum was selected using a 550 nm bandpass filter (Thorlabs). To ensure blockage of Rayleigh scattered photons, a 514 nm long-pass filter (Semrock #BLP01−514R-25) was used in conjunction with the bandpass filters. Typically, an EM camera gain setting of 500 was used for Raman images and zero for Rayleigh measurements with the same integration times.

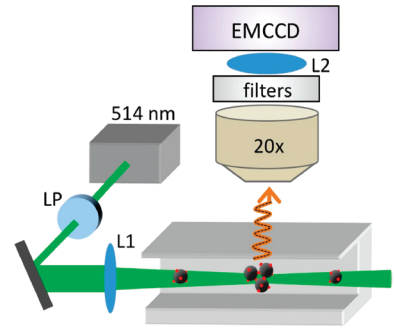

Figure 1. Schematic of setup used for dynamic SERS imaging. The collimated output from a 514 nm laser is passed through a laserline filter (LP), a PCX lens (f = 20 cm, L1), and directed through a simple channel enclosed by glass coverslips at each end and on the channel roof. The sample cell is mounted on a microscope stage with a 20× objective lens focused into the channel in the vicinity of the laser beam focus. An additional relay lens (L2) prior to the EMCCD was used along with different filters depending on whether Rayleigh or Raman scattering images were being acquired.

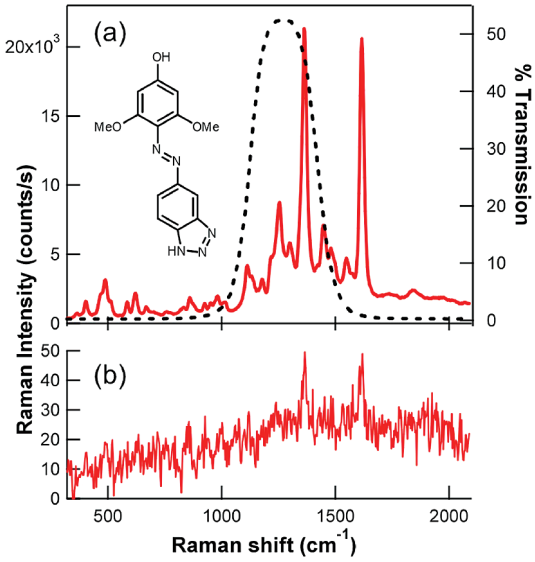

Figure 2. Ensemble SERS measurements (with no background correction) of 3,5-dimethoxy-4-(6′-azobenzotriazoyl)phenol (ABT-DMOP) at a concentration of 5 × 10^{-7} M (a) following $MgSO_4$-induced aggregation of the Ag colloid, and (b) prior to aggregation. Accumulation time = 1 s. The dotted line in (a) represents the transmission spectrum of a 550 nm bandpass filter used to select a portion of the Raman spectrum. The insert shows the structure of the ABT-DMOP reporter molecule.

Image Analysis. Additional Rayleigh-based image and tracking analysis was performed using a Nanosight LM10 instrument and accompanying Nanoparticle Tracking Analysis (NTA) software version 2.0. Videos up to 2 min long captured using either the EMCCD (SERS/Rayleigh) or LM10 (Rayleigh scattering) were analyzed using the NTA software. Further video and image processing was performed using *ImageJ*.

Results and Discussion

Prior to performing dynamic imaging measurements, nanoparticle clusters were first created via the $MgSO_4$-induced aggregation of a colloidal solution of Ag nanoparticles in the presence of 3,5-dimethoxy-4-(6′-azobenzotriazoyl) phenol (ABT-DMOP). This molecule (insert of Figure 2) was chosen as a SERS reporter based on previous work showing that the benzatriazole group strongly complexes to the silver surface by

displacing more weakly bound citrate anions as well as providing sharp, molecularly specific signals that can be uniquely identified in situ.[23] ABT-DMOP was first introduced to the Ag-citrate stock solution over a range of bulk concentrations followed by an incubation period of at least 30 min to ensure a steady-state surface coverage was achieved. Nanoparticle aggregation was then induced with the addition of $MgSO_4$ followed by SERS analysis. $MgSO_4$ results in a slower passive aggregation process when compared with NaCl as the sulfate anion is not thought to interact strongly with the particle surface and compete with the analyte for active sites.[26−28]

To emphasize the role of aggregation in greatly enhancing the SERS signal as well as discuss other possible signal contributions to the SERS images shown later, Figure 2 compares ensemble SERS spectra of ABT-DMOP before and after the addition of $MgSO_4$. The bulk concentration of ABT-DMOP was 0.5 μM at which a maximum SERS response was measured. At higher concentrations (>1 μM), a general decrease in the SERS signal was observed that is partly associated with destabilization of the nanoparticle colloid prior to salt introduction.[29] Accompanying UV−vis spectroscopy measurements were also performed (not shown here) with no significant red shift or broadening of the plasmon peak observed at concentrations below 10^{-6} M that could be attributed to ABT-DMOP-induced aggregation.

It is also important to note that the spectra in Figure 2 have not been background corrected. When imaging at a particular wavelength, it is possible that a significant fraction of the scattered photons are not attributable to SERS. However, it is clear from the low background signal in part b of Figure 2 and on comparing this with the dramatic increase in intensity observed after aggregation that any fluorescence contributions from ABT-DMOP are very small. This is expected as ABT-DMOP has an absorbance maximum at 425 nm in water and overlaps very weakly with the 514 nm excitation laser (Figure S1 of the Supporting Information). Thus only a very small component of the SERS enhancement will be associated with the molecular electronic resonance compared to the surface plasmon resonance enhancement. Furthermore, ABT-DMOP molecules adsorbed on the nanoparticle surface will be predominantly quenched. Other possible contributors to the background continuum, such as luminescence from the nanoparticles themselves, remain under debate, and to further improve the selectivity and contrast of the SERS image measurements a 550 nm bandpass filter was used to select a part of the spectrum. In the future, even narrower filters with higher transmittance will be employed.

Figure 3 compares representative Rayleigh scattering and SERS snapshot images acquired for both unaggregated and aggregated colloid at an ABT-DMOP concentration of 5×10^{-7} M. It can be clearly seen that in the absence of $MgSO_4$ very little SERS activity is observed with an average of less than one particle per frame over an extended video acquisition period of several minutes. This also indicates that there is sufficient blockage of Rayleigh scattered photons in the SERS image. However, upon aggregation, part b of Figure 3 shows that a significant fraction of the particles observed in the Rayleigh scattering image are now SERS active. To further confirm that the collected signal is attributable to SERS, additional control measurements were also performed. Figure 4 shows representative SERS images acquired when the 550 nm (1275 cm^{-1} shift) bandpass filter is replaced with one centered at 580 nm (2210 cm^{-1} shift) where there are no significant peaks in the SERS spectrum. The same aggregated colloid solution (5×10^{-7} M ABT-DMOP) and acquisition conditions are used in each case. Also, both images are plotted on the same intensity scale to enable a direct comparison. A significant reduction in both the particle image density and the cluster brightness can be clearly seen when the 580 nm filter is in place. Furthermore, in the absence of ABT-DMOP only a small percentage of clusters (<4%) formed upon aggregation remain visible under the SERS imaging conditions.

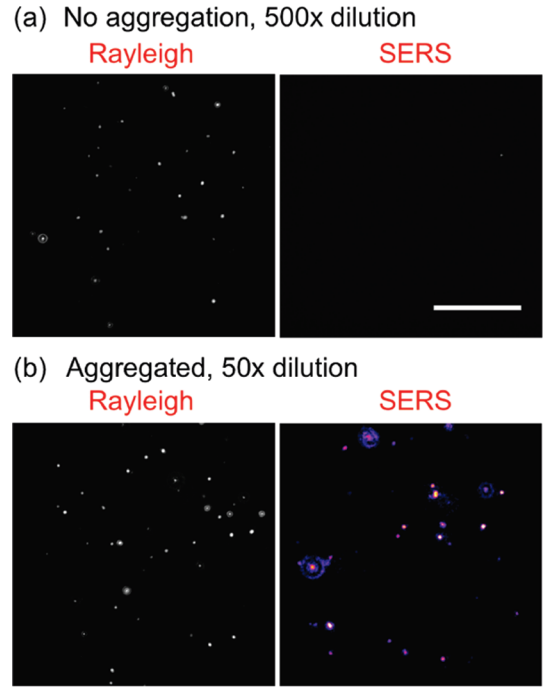

Figure 3. Comparison of representative Rayleigh and SERS image snapshots acquired at a ABT-DMOP concentration of 5×10^{-7} M. In (a) no salt was added to induce aggregation and the stock solution was diluted 500-fold in water prior to video acquisition. In (b) $MgSO_4$ was added followed by a 50-fold dilution in water. The scale bar in the upper right image represents 40 μm.

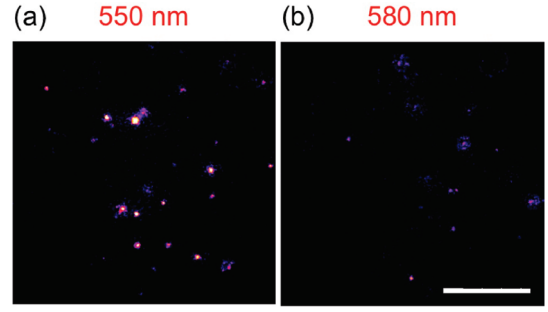

Figure 4. Representative SERS snapshot images of the same Ag colloid solution acquired with two different bandpass filters with center wavelengths of (a) 550 nm (1275 cm^{-1}) and (b) 580 nm (2215 cm^{-1}). A 514 nm long-pass filter was also used in both cases with the small difference in transmittance between the two bandpass filters also accounted for. Both images are plotted using the same false color intensity scale to allow direct comparison of signal intensities. The concentration of ABT-DMOP is 5×10^{-7} M and the scale bar in (b) represents 40 μm.

By comparing the average number of particles observed in each frame for a series of Rayleigh and SERS videos captured over several minutes it was possible to measure the fraction of clusters that were SERS active. To achieve this, both aggregated and unaggregated sample solutions were diluted 50-fold and 500-fold respectively immediately prior to imaging analysis. At lower particle densities (<10^9 per ml), changes in the average

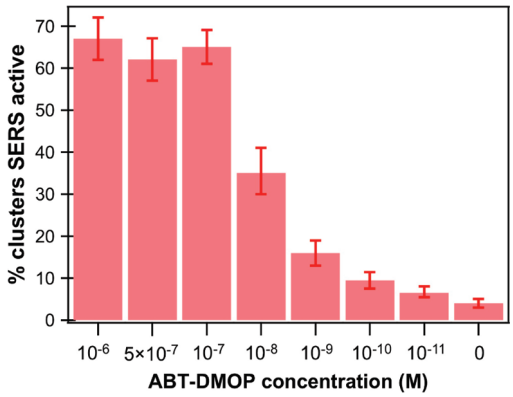

Figure 5. Measurement of the percentage of nanoparticle clusters formed in the presence of different bulk concentrations of ABT-DMOP that demonstrate significant SERS activity following $MgSO_4$-induced aggregation.

number of particles imaged at any one time were found to be directly proportional to any further reductions in the particle bulk concentration. This enables an accurate assessment of the fraction of particles observed by Rayleigh scattering that are actually SERS active. Another advantage is that the dilution process significantly slows further aggregation improving the reproducibility of repeat measurements. Also, at higher particle concentrations, background contributions to the image and increased crowding make effective particle tracking more difficult.

In the example in part b of Figure 3, the average number of clusters observed by Rayleigh scattering over 300 frames was 50.2, whereas the average number observed by SERS imaging was 32.5. This indicates that at least 65% of the nanoparticle aggregates formed were sufficiently bright to be imaged when the 514 nm long-pass and 550 nm bandpass filters were placed in front in front of the EMCCD. On performing repeat measurements at the same ABT-DMOP concentration of 5×10^{-7} M, the percentage of SERS active clusters was found to vary between 57 and 68%. The EMCCD integration time used here was 50 ms (for both Rayleigh and SERS image acquisition) because at higher integration times there was no apparent increase in particle density per frame in the SERS and Rayleigh images.

Figure 5 shows a series of results where the concentration of ABT-DMOP added to a fixed volume of Ag nanoparticle stock solution was systematically varied from 1 μM to 10 pM. At concentrations greater than 10^{-7} M the percentage of SERS active clusters measured were found to be similar. This is also consistent with the ensemble SERS measurements described above indicating that the fractional surface coverage of the Raman reporter adsorbate is approaching a full monolayer at this concentration range. At lower concentrations ($<10^{-7}$ M), the percentage of SERS active clusters formed starts to quickly decrease, which is expected because the probability of ABT-DMOP molecules being located in the vicinity of interparticle hot-spots within the aggregate structure will also decrease at lower surface coverages. It is clear that the SERS response does not follow a typical Langmuir isotherm with the drop in signal at lower concentrations also dependent on the nanoparticle cluster formation. In addition, when no ABT-DMOP is introduced, control experiments showed that a very small percentage of aggregates (typically 1−2 per frame) could still be observed. These aggregates have much larger Rayleigh scattering and/or background luminescence cross sections than average since the associated signal must be sufficiently bright to be observed

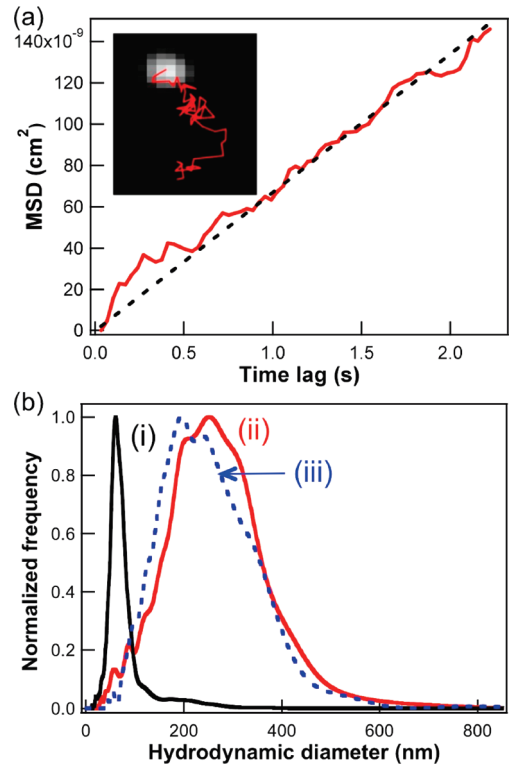

Figure 6. (a) 2D trajectory (insert) of an individual SERS-active cluster in solution is shown along with a plot of the mean square displacement (MSD) as a function of time and a linear regression fit. (b) Normalized size distributions obtained from Rayleigh imaging tracking of hundreds of nanoparticles before (i) and after (ii) salt-induced aggregation. The third distribution (iii) was obtained from a dynamic SERS analysis. In each case, the colloid samples were diluted as described previously in Figure 3 prior to analysis.

through the filters. For each measurement in Figure 5, it is likely that the percentages reported represent a minimum estimate since very weak SERS scatterers will not be observed.

In addition to investigating the SERS activity of individual clusters, the wide-field imaging approach is capable of separately monitoring the diffusional dynamics of up to ~100 particles or aggregates simultaneously to provide a powerful platform from which a profile of the particle size distribution can be quickly obtained. The x and y displacement of the centroid location of each nanoparticle between frames is tracked to enable the mean-square displacement (MSD) to be calculated from the resulting particle trajectory and plotted as a function of the time lag, τ. Under normal Brownian motion in solution where measurements are acquired in two dimensions, a linear relationship between MSD and τ is expected whose slope is equal to $4D$, where D is the particle diffusion coefficient.[30] The hydrodynamic diameter of the particle being tracked can then be obtained using the Stokes−Einstein relation, $D = k_bT/(6\pi\eta R)$, where k_b is the Boltzmann constant, T is the absolute temperature, η is the effective viscosity of the suspension medium, and R is the particle hydrodynamic radius.[31] The latter parameter assumes a spherical shape, which diffuses at the same speed as the cluster or individual particle. An example of dynamic SERS imaging analysis is demonstrated in part a of Figure 6 where the centroid position of a single SERS-active cluster was tracked at a frame rate of 29 Hz (2 ms EMCCD integration). The MSD plot calculated from the $x-y$ trajectory was fitted with a linear least-squares regression to establish a diffusion coefficient of 1.67×10^{-8} cm^2 s^{-1}. Using this value, the diameter of the nanoparticle cluster was found to be 270 nm using a viscosity of 0.955 mPa·s at a temperature of 22 °C.

A series of Rayleigh and SERS videos were then acquired in order to create size-distribution profiles of the Ag colloid both before and after aggregation. The first plot (i) in part b of Figure 6 is the Rayleigh analysis of diluted stock solution with the observed peak at 60 nm in excellent agreement with scanning electron microscopy characterization of the Ag colloid which revealed an average particle diameter of 56 nm (Figure S2 of the Supporting Information for representative SEM images). The weak tail present in the size distribution (i) toward 200 nm is due to the presence of a small fraction of nonspherical larger particles typical of the synthesis process as well as a low percentage of aggregates. While expected, this would not be apparent in conventional solution-based sizing techniques such as dynamic light scattering which do not operate on a particle by particle basis.

When the colloid was then aggregated the Rayleigh-based measurements in plot (ii) of part b of Figure 6 clearly show that the vast majority of clusters formed have an approximate diameter between 150 and 350 nm and only a very small fraction of particles remain unaggregated. This distribution range was observed reproducibly after developing a procedure where the colloid was diluted 50-fold with water within a few seconds of $MgSO_4$ addition prior to image analysis. Under these conditions, the rate of further aggregation is significantly slowed thus reducing the formation of much larger aggregates during the measurement time scale that would occur in the undiluted stock solution. The measured size distribution suggests an average of 3−12 particles are involved in each cluster. Also, comparison of Rayleigh videos using the dilution conditions described in Figure 3 support a ∼8-fold reduction in particle density upon aggregation. This would have been difficult to deduce using other characterization techniques such as electron microscopy measurements where achieving a substrate that is representative of the aggregated colloid solution is difficult. In a previous study by Khan et al.,[10] SERS maps and electron microscopy images of Ag clusters were correlated with the percentage of SERS active clusters and reported to be as high as 50−60% for aggregates containing 2−9 particles. Also, all larger clusters (>10 particles) exhibited some degree of activity although the total number of clusters actually studied was very limited.

The final curve (iii) in part b of Figure 6 is the size profile obtained from SERS videos using the setup described previously in Figure 1. At the faster frame rate and lower integration time used here compared to the data in Figure 3, the fraction of SERS active particles visible at any one time will be lower. However, this is in part compensated for by analyzing several hundred particles in order to create a size profile. Both curves (i) and (ii) in part b of Figure 4 were obtained using a Nanosight LM10 instrument, which has a slightly different optical configuration (ref 32) than that described in Figure 1, which was used to generate both curve (iii) and each image in Figures 3 and 4. The key difference is the focusing of the laser directly into the channel for the Raman measurements rather than coupling into the solution via a glass prism and focusing at a short distance above the prism surface. Depending on the location of the beam focus with respect to the objective lens, a net lateral or vertical movement of nanoparticles can be observed due to radiation pressure creating a gradient force. In the case here, a relatively gentle beam focus was employed (unlike the conditions required for optical trapping[33,34]) and the SERS and Rayleigh imaging measurements performed in a region where net flow was minimal. Furthermore, the NTA analysis software can identify and account for the presence of an average net flow superimposed on the Brownian motion pattern of each individual particle. The success of these proof-of-principle measurements is supported by the relatively good agreement between curves (ii) and (iii) in part b of Figure 6.

Finally, in an ideal system it would also be possible to directly confirm which size of nanoparticle cluster on average produced the brightest SERS signal. This is difficult as each cluster quickly diffuses across the laser beam profile through the focal plane and depends on a potentially large number of experimental factors. In the dynamic SERS measurements described in Figure 6, no strong correlation was observed where, for example, the maximum SERS pixel intensity (which varied over 1−2 orders of magnitude) was consistently lower for smaller clusters compared to larger clusters. Recently, Tay et al. reported measurements on adsorbate saturated nanoparticles immobilized on a substrate where no overall increase in SERS intensity was observed at larger aggregate sizes.[35] The Van Duyne group have also shown the SERS enhancement to be crucially dependent on the interparticle gap rather than on the aggregation state itself.[36] Work is currently underway to further improve the level of characterization and achieve higher discrimination between different cluster sizes such as dimers and trimers through a combination of optical design, additional software analysis tools, and greater control of the aggregation process. It is expected the flexibility of this dynamic imaging approach will enable studies involving a wide range of nanoparticle types and different nanoparticle-enhanced spectroscopies.

Summary

A simple and effective imaging-based approach capable of identifying and dynamically tracking individual SERS-active nanoparticle clusters suspended in solution has been demonstrated. The ability to measure simultaneously the diffusion coefficient of hundreds of individual particles and clusters and compare videos using both the Rayleigh scattering and SERS imaging modalities is particularly powerful. As a result, we were able to directly measure in situ the fraction of clusters formed upon salt-induced aggregation, which demonstrated significant SERS activity. To our knowledge, this is also the first demonstration of the dynamic imaging of rapidly moving nanoparticles via a SERS modality; which opens up new opportunities for fundamental studies of SERS and nanoparticle aggregation, single molecule SERS studies, as well as the more precise engineering of uniformly responsive SERS substrates. Furthermore, we envision that the dynamic imaging system described here represents an important step in the creation of the next generation of ultrasensitive biosensors by moving away from the inherent limitations associated with bulk solution measurements and toward a simple, high-throughput single nanoparticle analysis platform.

Acknowledgment. This work was supported by an Engineering Physical Sciences Research Council (EPSRC) Science and Innovation Award and an EPSRC First Grant award (#EP/H030468/1). We also thank Dr Patrick Hole and Dr Bob Carr of Nanosight Ltd for support and useful discussions.

Supporting Information Available: Additional characterization data of the colloid and ABT-DMOP. This material is available free of charge via the Internet at http://pubs.acs.org.

References and Notes

(1) Graham, D.; Faulds, K. *Chem. Soc. Rev.* **2008**, *37*, 1042.
(2) Kneipp, K.; Wang, Y.; Kneipp, H.; Perelman, L. T.; Itzkan, I.; Dasari, R. R.; Feld, M. S. *Phys. Rev. Lett.* **1997**, *78*, 1667.

(3) Etchegoin, P. G.; Le Ru, E. C. *Phys. Chem. Chem. Phys.* **2008**, *10*, 6079.
(4) Faulds, K.; McKenzie, F.; Smith, W. E.; Graham, D. *Angew. Chem., Int. Ed.* **2007**, *46*, 1829.
(5) Qian, X.; Peng, X.-H.; Ansari, D. O.; Yin-Goen, Q.; Chen, G. Z.; Shin, D. M.; Yang, L.; Young, A. N.; Wang, M. D.; Nie, S. *Nat. Biotechnol.* **2008**, *26*, 83.
(6) Martin, L. C.; Larmour, I. A.; Faulds, K.; Graham, D. *Chem. Commun.* **2010**, *46*, 5247.
(7) McHugh, C. J.; Keir, R.; Graham, D.; Smith, W. E. *Chem. Commun.* **2002**, 580.
(8) Cunningham, D.; Littleford, R. E.; Smith, W. E.; Lundahl, P. J.; Khan, I.; McComb, D. W.; Graham, D.; Laforest, N. *Faraday Discuss.* **2006**, *132*, 135.
(9) Chen, G.; Wang, Y.; Yang, M.; Xu, J.; Goh, S. J.; Pan, M.; Chen, H. *J. Am. Chem. Soc.* **2010**, *132*, 3644.
(10) Khan, I.; Cunningham, D.; Littleford, R. E.; Graham, D.; Smith, W. E.; McComb, D. W. *Anal. Chem.* **2006**, *78*, 224.
(11) Talley, C. E.; Jackson, J. B.; Oubre, C.; Grady, N. K.; Hollars, C. W.; Lane, S. M.; Huser, T. R.; Nordlander, P.; Halas, N. J. *Nano Lett.* **2005**, *5*, 1569.
(12) Camden, J. P.; Dieringer, J. A.; Wang, Y.; Masiello, D. J.; Marks, L. D.; Schatz, G. C.; Van Duyne, R. P. *J. Am. Chem. Soc.* **2008**, *130*, 12616.
(13) Laurence, T. A.; Braun, G.; Talley, C.; Schwartzberg, A.; Moskovits, M.; Reich, N.; Huser, T. *J. Am. Chem. Soc.* **2009**, *131*, 162.
(14) Sebba, D. S.; Watson, D. A.; Nolan, J. P. *ACS Nano* **2009**, *3*, 1477.
(15) Goddard, G.; Brown, L. O.; Habbersett, R.; Brady, C. I.; Martin, J. C.; Graves, S. W.; Freyer, J. P.; Doorn, S. K. *J. Am. Chem. Soc.* **2010**, *132*, 6081.
(16) Bingham, J. M.; Willets, K. A.; Shah, N. C.; Andrews, D. Q.; Van Duyne, R. P. *J. Phys. Chem. C* **2009**, *113*, 16839.
(17) Xu, C. S.; Cang, H.; Montiel, D.; Yang, H. *J. Phys. Chem. C* **2007**, *111*, 32.
(18) Nallathamby, P. D.; Lee, K. J.; Xu, X.-H. N. *ACS Nano* **2008**, *2*, 1371.
(19) Thompson, M. A.; Lew, M. D.; Badieirostami, M.; Moerner, W. E. *Nano Lett.* **2010**, *10*, 211.
(20) Pinaud, F.; Clarke, S.; Sittner, A.; Dahan, M. *Nat. Methods* **2010**, *7*, 275.
(21) Schluecker, S.; Schaeberle, M. D.; Huffman, S. W.; Levin, I. W. *Anal. Chem.* **2003**, *75*, 4312.
(22) Stokes, R. J.; McKenzie, F.; McFarlane, E.; Ricketts, A.; Tetley, L.; Faulds, K.; Alexander, J.; Graham, D. *Analyst* **2009**, *134*, 170.
(23) McAnally, G.; McLaughlin, C.; Brown, R.; Robson, D. C.; Faulds, K.; Tackley, D. R.; Smith, W. E.; Graham, D. *Analyst* **2002**, *127*, 838.
(24) Lee, P. C.; Meisel, D. *J. Phys. Chem.* **1982**, *86*, 3391.
(25) Munro, C. H.; Smith, W. E.; Garner, M.; Clarkson, J.; White, P. C. *Langmuir* **1995**, *11*, 3712.
(26) Bell, S. E. J.; Sirimuthu, N. M. S. *J. Phys. Chem. A* **2005**, *109*, 7405.
(27) Bell, S. E. J.; Sirimuthu, N. M. S. *J. Am. Chem. Soc.* **2006**, *128*, 15580.
(28) Larmour, I. A.; Faulds, K.; Graham, D. *J. Phys. Chem. C* **2010**, *114*, 13249.
(29) McLaughlin, C.; Graham, D.; Smith, W. E. *J. Phys. Chem. B* **2002**, *106*, 5408.
(30) Saxton, M. J. *Biophys. J.* **1997**, *72*, 1744.
(31) Crocker, J. C.; Grier, D. G. *J. Colloid Interface Sci.* **1996**, *179*, 298.
(32) Montes-Burgos, I.; Walczyk, D.; Hole, P.; Smith, J.; Lynch, I.; Dawson, K. *J. Nanopart. Res.* **2010**, *12*, 47.
(33) Dholakia, K.; Reece, P.; Gu, M. *Chem. Soc. Rev.* **2008**, *37*, 42.
(34) Svedberg, F.; Li, Z.; Xu, H.; Kall, M. *Nano Lett* **2006**, *6*, 2639.
(35) Tay, L.-L.; Hulse, J.; Kennedy, D.; Pezacki, J. P. *J. Phys. Chem. C* **2010**, *114*, 7356.
(36) Wustholz, K. L.; Henry, A.-I.; McMahon, J. M.; Freeman, R. G.; Valley, N.; Piotti, M. E.; Natan, M. J.; Schatz, G. C.; Van Duyne, R. P. *J. Am. Chem. Soc.* **2010**, *132*, 10903.

JP107559X